

# UNOPose: Unseen Object Pose Estimation with an Unposed RGB-D Reference Image

Xingyu Liu<sup>1,\*</sup>, Gu Wang<sup>1,\*</sup>, Ruida Zhang<sup>1</sup>,  
Chenyanguang Zhang<sup>1</sup>, Federico Tombari<sup>2,3</sup>, and Xiangyang Ji<sup>1</sup>  
<sup>1</sup>Tsinghua University, <sup>2</sup>Technical University of Munich, <sup>3</sup>Google

{liuxy21@mails., wanggu1@, zhangrd23@mails., zcyg22@mails., xyji@}tsinghua.edu.cn,  
tombari@in.tum.de

## Abstract

*Unseen object pose estimation methods often rely on CAD models or multiple reference views, making the onboarding stage costly. To simplify reference acquisition, we aim to estimate the unseen object’s pose through a single unposed RGB-D reference image. While previous works leverage reference images as pose anchors to limit the range of relative pose, our scenario presents significant challenges since the relative transformation could vary across the entire  $SE(3)$  space. Moreover, factors like occlusion, sensor noise, and extreme geometry could result in low viewpoint overlap. To address these challenges, we present a novel approach and benchmark, termed UNOPose<sup>1</sup>, for UNseen One-reference-based object Pose estimation. Building upon a coarse-to-fine paradigm, UNOPose constructs an  $SE(3)$ -invariant reference frame to standardize object representation despite pose and size variations. To alleviate small overlap across viewpoints, we recalibrate the weight of each correspondence based on its predicted likelihood of being within the overlapping region. Evaluated on our proposed benchmark based on the BOP Challenge, UNOPose demonstrates superior performance, significantly outperforming traditional and learning-based methods in the one-reference setting and remaining competitive with CAD-model-based methods. The code and dataset will be available.*

## 1. Introduction

Localizing an object in Euclidean space by estimating its 6DoF pose, *i.e.*, 3DoF orientation and 3DoF position, plays a crucial role in augmented/virtual reality [52, 69], scene understanding [31, 56] and robotic manipulation [18, 72]. The vast majority of works [36, 42, 61, 74, 75] focuses on instance-level object pose estimation, where the training and

testing datasets consist of an identical set of known object instances, and the CAD models of objects are often required for generating training images and labels. More recently, Wang *et al.* [76] and its successors [6, 71, 77] extended this paradigm to the category level, intending to estimate poses for novel instances within predefined categories without requiring CAD models of target objects. Both paradigms have limitations in open-world applications, where annotating and training for new objects beyond known categories would be very labor-intensive and sometimes prohibitive.

To mitigate this problem, recent research efforts [3, 37, 46, 79] have shifted towards pose estimation of arbitrary novel objects, where the target object is unseen during training. This task presents a great challenge due to the inherent uncertainty of the novel object’s canonical frame (defined in the CAD model of the object). Current approaches [37, 50, 55] often tackle this by using omnidirectional reference views to cover the target object, separating pose estimation task to viewpoint selection and relative pose estimation to known pose anchors. If CAD models are available during the test phase, reference views can be easily produced through image rendering [37, 46, 54, 79]. Alternatively, without CAD models, reference views can be obtained by capturing multiple images of the object [23, 25, 70]. Both setups have shortcomings, as creating a CAD model of an object or labeling a substantial number of object poses is limited in scalability. For example, they can hardly adapt to in-the-wild scenarios where novel objects are introduced unpredictably.

To sum up, while existing methods exhibit promising transfer capability to novel objects, they are notably constrained by their reliance on the CAD model or multiple reference views (Fig. 1 (a, b)). In this work, we aim to minimize onboarding cost by estimating novel object poses using a single unposed RGB-D reference image (Fig. 1). This setup is different from existing methods mainly in two aspects. First, we focus on estimating the relative pose between two unposed viewpoints rather than the absolute pose.

\*Equal contributions.

<sup>1</sup>UNO (/ˈuːnɒs/) means one in Spanish and Italian.

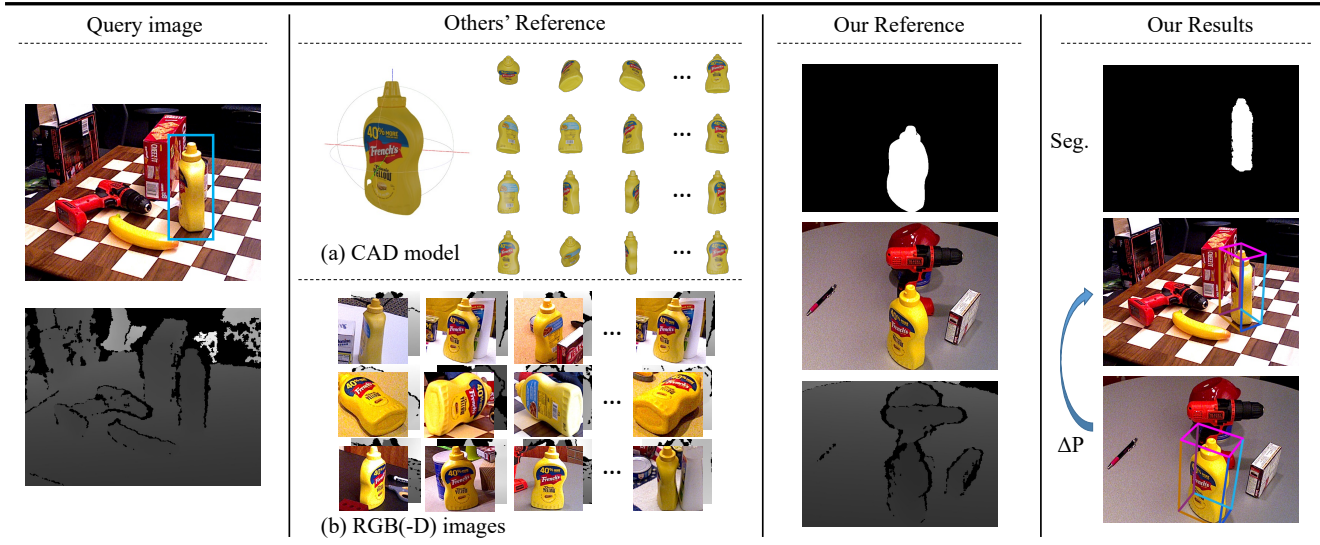


Figure 1. **Illustration of unseen object pose estimation.** Given a query image presenting a target object unseen during training, we aim to estimate its segmentation and 6DoF pose w.r.t. a reference frame. While previous methods [37, 50, 70, 79] often rely on the CAD model or multiple RGB(-D) images for reference, we merely use one unposed RGB-D reference image.

Note that the absolute pose of a novel object becomes ill-posed without a certain canonical frame, while relative pose estimation remains well-defined regardless of the canonical frame’s definition. Secondly, some existing relative pose estimation methods [87, 91, 92] merely use RGB modality to predict the 3DoF rotation. These methods have limited ability to predict relative translation and generalize beyond their training datasets. In contrast, we fully leverage RGB-D modality to predict the 6DoF relative pose, meanwhile enhancing the network’s generalizability to novel objects and environments.

Nevertheless, estimating the pose of unseen objects with only one reference view presents significant challenges from various aspects. First, previous methods [3, 37, 79] select the most similar reference view as a pose anchor, distinctly reducing the search space for relative poses. However, in our scenario, where both the target and reference object poses are unknown, the relative pose can vary across the entire  $SE(3)$  space. Moreover, in partial-to-partial object matching, factors such as occlusion, sensor noise, and extreme geometry can severely interfere with the matching process. To address these challenges, we propose a novel approach and benchmark for *UNseen One-reference-based object Pose estimation (UNOPose)*. Our pipeline leverages the strong generalization capabilities of vision foundation models [34, 58] to produce an effective segmentation of the unseen object. Then, UNOPose employs a coarse-to-fine paradigm for estimating the relative pose between the reference and the query objects. To alleviate the challenge of diverse pose and size variations, we introduce the  $SE(3)$ -invariant global reference frame (*GRF*) to standardize object

representation. Subsequently, a hierarchical object encoding paradigm based on the local reference frame (*LRF*) further captures fine-grained geometric details. For achieving reliable correspondences in partial-to-partial object matching, we harness an overlap predictor to identify and concentrate on the overlapping region.

Moreover, we propose a new benchmark devised from the BOP challenge [28] to facilitate evaluation and future research of unseen object pose estimation with one reference. Extensive experiments on YCB-V [81], LM-O [2] and TUD-L [26] datasets demonstrate that our UNOPose surpasses all compared methods on a single reference setting. To our surprise, UNOPose with an unposed reference is even on par with some  $SE(3)$ -invariant-feature-based methods relying on CAD models (Ours 70.9% vs. ZTE-PPF [1] 69.0% vs. Koenig-PPF [35] 75.1% w.r.t.  $AR_{BOP}$  metric).

Our contributions can be summarized as follows:

- To the best of our knowledge, we are the first to conduct unseen object 6DoF pose estimation leveraging a single unposed RGB-D reference.
- Based on the BOP Challenge, we devise a new extensive benchmark tailored for unseen object segmentation and pose estimation with one reference. Additionally, we evaluate several traditional and learning-based methods on this benchmark for completeness.
- We introduce UNOPose, a network for learning relative transformation between reference and query objects. To achieve this, we propose the  $SE(3)$ -invariant global and local reference frames, enabling standardized object representations despite variations in pose and size. Furthermore, the network can automatically adjust the

confidence of each correspondence by incorporating an overlap predictor.

## 2. Related Work

**Class-specific Pose Estimation.** Class-specific object pose estimation aims at predicting 6DoF poses of either instance of a known object (instance-level) or unseen objects within a known category (category-level). Instance-level object poses are often solved by direct regression [29, 41, 75] using deep neural networks, or by establishing 2D-3D [21, 42, 61] or 3D-3D correspondences [24, 66, 74] which are then leveraged by RANSAC-based PnP/Kabsch algorithms. The instance-level setting requires expensive data generation/annotation and training for every new object. To address this limitation, category-level pose estimation [76] is proposed to estimate 9DoF poses of novel objects among specific categories without CAD models. Mainstream approaches can also be categorized into direct regression [6, 9, 44, 45, 49, 88] or correspondence-based [8, 19, 71, 76] methods. However, this setting remains constrained to a limited number of categories, given the additional challenge of aligning canonical frames, managing symmetric objects, and categorizing objects in similar categories correctly (*e.g.* can and bottle).

**Novel Object Pose Estimation.** Estimating the pose of novel objects beyond known classes, *i.e.*, objects at inference time are unseen during training, is a useful yet challenging task. Existing works solve this problem through image-based matching [3, 37, 53, 54, 67, 79, 90] or feature-based matching approaches [4, 23, 30, 46, 55, 59, 70]. Notably, given a target image, OVE6D [3] and MegaPose [37] retrieve the most similar viewpoint from a pre-rendered omnidirectional image database as a coarse pose estimate. A customized neural network then refines the coarse pose estimate. FoundationPose [79] further builds a pose ranking network to score each refined pose hypothesis. Feature-matching methods learn local feature descriptors to construct pixel-level or point-level correspondences. For example, OnePose [70] and OnePose++ [23] reconstruct the 3D point cloud of an unseen object to establish 2D-3D correspondences, whereas SAM-6D [46] builds 3D-3D correspondences. More recently, some methods [4, 59] directly exploit the power of foundation models for zero-shot pose estimation. Exemplarily, FoundPose [59] extracts DINOv2 visual features [58], while FreeZe [4] further utilizes generalizable geometric features [62] to conduct feature matching.

**Relative Pose Estimation.** Orthogonal to previous works which rely on known instances or multiple reference views, relative object pose estimation estimates a relative transformation of the unseen object with only one reference image. One closely related topic is camera pose estimation from two views. For example, RelPose [87] and RelPose++ [43] infer a distribution of relative rotations by leveraging an energy-based formulation. Moreover, iFusion [80] optimizes the

unknown relative pose by inverting the novel view synthesis diffusion model [48]. Relative camera pose estimation relies on static background to establish correspondence between viewpoints. In the field of relative object pose estimation, given two RGB images, 3DAHV [91] presents a hypothesis-and-verification framework to score each relative pose hypothesis. Extended by that, DVMNet [92] introduces a hypothesis-free pipeline to compute relative poses via deep voxel matching. The above works have limited capability in inferring 3DoF relative translations. In this work, with the introduction of depth data, we can estimate a complete 6DoF pose including rotation and translation.

**Point Cloud Registration.** Our approach follows the paradigm of correspondence-based methods [13, 14, 39, 78], which initially extract 3D local feature descriptors to establish correspondences between source and target point clouds. Subsequently, they estimate the relative transformation using techniques like SVD, RANSAC, or Hough Voting [38]. Some feature descriptors are proposed to ensure rotational invariance. For example, FPFH [65] descriptor is computed with geometric surface properties. PPF [17] uses the distance and angles to describe the relation of point pairs. TOLDI [82] proposes a robust local reference frame using keypoint normals and neighboring projections. With the advent of deep learning, neural networks are increasingly employed to extract 3D local or global feature descriptors [11, 32, 64, 78, 86].

## 3. UNO Object Segmentation and Pose Estimation

### 3.1. Problem Formulation

Assuming an arbitrary unseen rigid object in a query image, our goal is to estimate the object’s mask  $M_q$  and its 6DoF relative pose  $\Delta\mathbf{T} \in SE(3)$  with a masked RGB-D reference image exhibiting the target object without major occlusion or truncation. As illustrated in Fig. 1, the input is:

- 1)  $[I_q|D_q] \in \mathbb{R}^{H \times W \times 4}$ : The query RGB-D image;
- 2)  $[I_p|D_p] \in \mathbb{R}^{H \times W \times 4}$  and  $M_p \in \mathbb{R}^{H \times W}$ : The reference RGB-D image and the corresponding binary mask indicating the target object;
- 3)  $K_q \in \mathbb{R}^{3 \times 3}$  and  $K_p \in \mathbb{R}^{3 \times 3}$ : Camera intrinsics of the query and reference images.

Optionally, if the pose  $\mathbf{T}_p \in SE(3)$  of the reference object in the camera frame is known, the query object pose  $\mathbf{T}_q \in SE(3)$  can be recovered by  $\mathbf{T}_q = \Delta\mathbf{T}\mathbf{T}_p$ . Note that, for practicality, the method should not rely on the absolute pose of the reference object, since the world frame can vary arbitrarily in different applications. We only use the reference object pose during the inference stage for evaluation on standard object pose datasets.

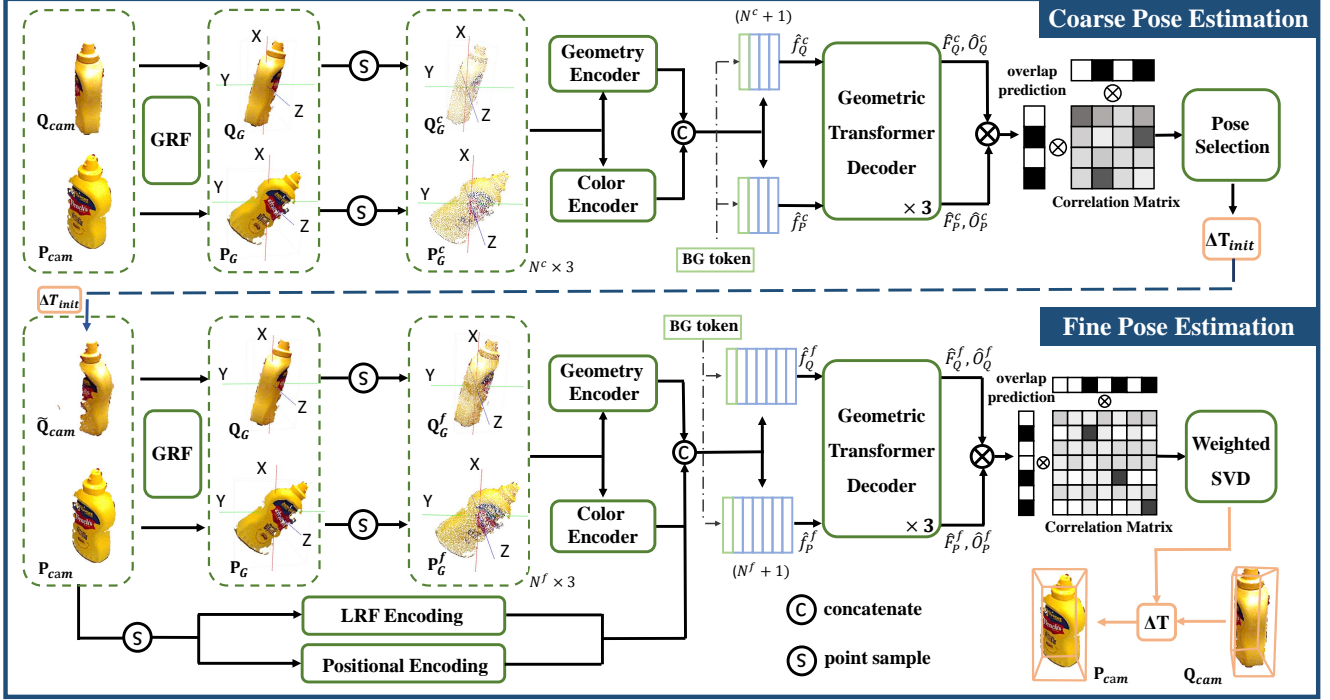


Figure 2. **The network architecture of UNOPose.** Given the query and reference point clouds  $\mathbf{Q}_{cam}$  and  $\mathbf{P}_{cam}$  in the camera frame, UNOPose first transforms them into the  $SE(3)$ -invariant global reference frame (GRF). Then feature descriptors are extracted from sparse point sets for constructing the coarse correlation matrix. For achieving precise correspondences, the fine pose estimation module exploits structural details using positional encoding and local reference frame (LRF) encoding.

### 3.2. UNO Object Segmentation

Firstly, we segment the query object from a cluttered background. Thanks to the great generalization ability of vision foundation models, methods like [7, 46, 54] can effectively segment novel objects with CAD models. However, unlike previous approaches, which generate diverse descriptors from multiple rendered views, we can access *only a single reference image*. To address this challenge, we use the SAM model [34] to predict all possible mask proposals from the query image, and then score each mask proposal by comparing DINOv2 [58] descriptors between the query and reference images using cosine similarity, identifying the most similar mask  $M_q$ . Please refer to supplementary materials for more details about UNO segmentation.

### 3.3. UNO Object Pose Estimation

#### 3.3.1. Overview of UNOPose

Given the predicted mask  $M_q$  of the query image and mask  $M_p$  of the reference image, we crop and back-project the object of interest from depth maps  $D_q, D_p$  into the camera space as two point sets  $\mathbf{Q}_{cam} \in \mathbb{R}^{N^Q \times 3}$  and  $\mathbf{P}_{cam} \in \mathbb{R}^{N^P \times 3}$ , where  $N^Q$  and  $N^P$  denotes the point numbers of query and reference point clouds, respectively. Our goal is to recover the relative transformation  $\Delta \mathbf{T} = \{\Delta \mathbf{R}, \Delta \mathbf{t}\}$  by

minimizing the correspondence distance

$$\min_{(\mathbf{q}, \mathbf{p}) \in \mathbf{C}} \|\Delta \mathbf{R} \mathbf{q} + \Delta \mathbf{t} - \mathbf{p}\|_2, \quad (1)$$

where  $\mathbf{C}$  is the predicted correspondence set between  $\mathbf{Q}_{cam}$  and  $\mathbf{P}_{cam}$ . We exploit both color and geometric cues to build this correspondence and follow the broadly used coarse-to-fine paradigm in point cloud registration to solve Eq. (1). The network is demonstrated in Fig. 2.

#### 3.3.2. Coarse-to-fine Pose Estimation

**Constructing a Pose-invariant Reference Frame.** Given only an unposed reference image, the relative pose to predict is arbitrary in the whole  $SE(3)$  space, which renders a significant challenge for achieving robust correspondences. Hence, we introduce a pose-invariant global reference frame (GRF) and transform  $\mathbf{Q}_{cam}$  and  $\mathbf{P}_{cam}$  into GRF as  $\mathbf{Q}_G$  and  $\mathbf{P}_G$ .

Concretely, taking  $\mathbf{Q}_{cam}$  as an example, transforming the point cloud to GRF involves a 7DoF coordinate transformation  $\{\mathbf{R}_G \in SO(3), \mathbf{t}_G \in \mathbb{R}^3, s_G \in \mathbb{R}\}$ :

$$\mathbf{Q}_G = \{\mathbf{R}_G^T(\mathbf{q} - \mathbf{t}_G)/s_G \mid \mathbf{q} \in \mathbf{Q}_{cam}\}. \quad (2)$$

The origin of GRF is located at the object center  $\mathbf{c}_Q$  for translation invariance, and the radius of the point cloud is

rescaled to 1 for size invariance, computed as

$$\mathbf{t}_G = \mathbf{c}_Q, \quad s_G = \max_{\mathbf{q} \in \mathbf{Q}_{cam}} \|\mathbf{q} - \mathbf{c}_Q\|_2. \quad (3)$$

The key ingredient is to devise the rotation  $\mathbf{R}_G = [\mathbf{r}_{Gx} | \mathbf{r}_{Gy} | \mathbf{r}_{Gz}]$ , where  $\mathbf{r}_{Gx}, \mathbf{r}_{Gy}, \mathbf{r}_{Gz}$  are the three columns of  $\mathbf{R}_G$ , ensuring orientation invariance for the transformed point cloud. Inspired by former works [20, 68, 82], we use the normal vector of the object center  $\mathbf{n}(\mathbf{c}_Q)$  as  $\mathbf{r}_{Gz}$ , and project all points in  $\mathbf{Q}_{cam}$  onto the tangent plane of  $\mathbf{c}_Q$ , summarizing the projected vectors to determine  $\mathbf{r}_{Gx}$ . Then,  $\mathbf{r}_{Gy}$  is obtained by the cross-product of  $\mathbf{r}_{Gx}$  and  $\mathbf{r}_{Gz}$ , *i.e.*,  $\mathbf{r}_{Gy} = \mathbf{r}_{Gx} \times \mathbf{r}_{Gz}$ . This ensures that the XY-plane evenly divides the point cloud, with the x-axis representing the principal projection direction. The GRF is  $SE(3)$ -invariant as it can be uniquely determined by the spatial distribution of the point cloud, making the transformed point cloud robust to variations in pose and size.

Concretely, we perform SVD on the covariance matrix  $\text{Cov}(\mathbf{Q}_{cam}) = \frac{1}{N_Q} \mathbf{Q}_{cam}^\top \mathbf{Q}_{cam} - \mathbf{c}_Q \mathbf{c}_Q^\top$  and use the singular vector w.r.t. the minimum singular value to determine  $\mathbf{r}_{Gz}$ :

$$\mathbf{r}_{Gz} = \begin{cases} \mathbf{n}(\mathbf{c}_Q), & \text{if } \mathbf{n}(\mathbf{c}_Q)^\top \sum_{\mathbf{q} \in \mathbf{Q}_{cam}} (\mathbf{c}_Q - \mathbf{q}) > 0 \\ -\mathbf{n}(\mathbf{c}_Q), & \text{otherwise.} \end{cases} \quad (4)$$

Afterwards,  $\mathbf{r}_{Gx}$  is computed as

$$\mathbf{r}_{Gx} = \sum_{\mathbf{q} \in \mathbf{Q}_{cam}} w_q ((\mathbf{q} - \mathbf{c}_Q) - \mathbf{r}_{Gz}^\top (\mathbf{q} - \mathbf{c}_Q) \mathbf{r}_{Gz}), \quad (5)$$

where  $w_q$  is a weight w.r.t. distance between  $\mathbf{q}$  and  $\mathbf{c}_Q$  (See supplementary materials for details).

Previous works often depend on complex networks or computationally expensive PPF features for  $SE(3)$  invariance [40, 83, 85]. In contrast, our transformation is computationally efficient and can seamlessly adapt to a wide range of network architectures.

**Coarse Pose Estimation.** Given point clouds  $\mathbf{Q}_G$  and  $\mathbf{P}_G$  in GRF, we sample two sparse point sets  $\mathbf{Q}_G^c \in \mathbb{R}^{N^c \times 3}$  and  $\mathbf{P}_G^c \in \mathbb{R}^{N^c \times 3}$  to efficiently obtain a coarse pose initialization  $\Delta \mathbf{T}_{init}$ . Specifically, we leverage a geometry encoder [64] and a color encoder [58] to extract point cloud and RGB features separately. Features are further concatenated as  $f_Q^c \in \mathbb{R}^{N^c \times d}$  and  $f_P^c \in \mathbb{R}^{N^c \times d}$ , where  $d$  is the dimension of embeddings. Following [46], we add a learnable background token for assigning non-overlapping points. The embeddings, denoted as  $\hat{f}_Q^c \in \mathbb{R}^{(N^c+1) \times d}$  and  $\hat{f}_P^c \in \mathbb{R}^{(N^c+1) \times d}$ , are processed by three stacked Geometric Transformer decoding modules [64].

The outputs of the last decoder  $\hat{F}_Q^c \in \mathbb{R}^{(N^c+1) \times D}$  and  $\hat{F}_P^c \in \mathbb{R}^{(N^c+1) \times D}$  are point-wise features for building the correlation matrix. However, in our setting, the overlap ratio can be influenced by complicated factors like viewpoint,

occlusion or depth noise. To solve this issue, the network additionally predicts overlap confidences  $\hat{O}_Q^c \in \mathbb{R}^{(N^c+1) \times 1}$  and  $\hat{O}_P^c \in \mathbb{R}^{(N^c+1) \times 1}$ , which indicate point-wise probabilities of being in the overlapping region. The overlap-aware correlation matrix  $\mathbf{X}^c \in \mathbb{R}^{(N^c+1) \times (N^c+1)}$  can thus be computed by

$$\mathbf{X}^c = \text{softmax}[(\hat{O}_Q^c \odot \hat{F}_Q^c)(\hat{O}_P^c \odot \hat{F}_P^c)^\top]. \quad (6)$$

Here  $\odot$  indicates element-wise multiplication. Each element in  $\mathbf{X}^c$  suggests a correlation score between a point pair in  $\mathbf{Q}^c$  and  $\mathbf{P}^c$ .

Once  $\mathbf{X}^c$  is computed, we can extract all possible corresponding point pairs between  $\mathbf{Q}^c$  and  $\mathbf{P}^c$  as well as their correlation scores to solve Eq. (1). We first compute pose hypotheses by sampling  $N_H$  triplets of point pairs according to the distribution of  $\mathbf{X}^c$ . Then each pose hypothesis  $\Delta \mathbf{T}_h = \{\Delta \mathbf{R}_h, \Delta \mathbf{t}_h\}$  is scored with the reciprocal of distance  $D_h$  as in [21, 46]

$$D_h = \frac{1}{N^c} \sum_{\mathbf{p}^c \in \mathbf{P}^c} \min_{\mathbf{q}^c \in \mathbf{Q}^c} \|\Delta \mathbf{R}_h^\top (\mathbf{q}^c - \Delta \mathbf{t}_h) - \mathbf{p}^c\|_2, \quad (7)$$

$$\xi_h = \frac{1}{D_h}, \quad h = 1, 2, 3, \dots, N_H.$$

The pose hypothesis with the highest score  $\xi_h$  is selected as the initial pose prediction  $\Delta \mathbf{T}_{init} = \{\Delta \mathbf{R}_{init}, \Delta \mathbf{t}_{init}\}$  and further sent to transform the input of the next stage.

**Fine Pose Estimation.** After transforming  $\mathbf{Q}_{cam}$  to  $\tilde{\mathbf{Q}}_{cam}$  with the initial pose prediction  $\Delta \mathbf{T}_{init}$ , we perform a fine matching process between two dense point sets, *i.e.*,  $\tilde{\mathbf{Q}}^f \in \mathbb{R}^{N^f \times 3}$  and  $\mathbf{P}^f \in \mathbb{R}^{N^f \times 3}$ , to achieve a more accurate pose. The network exploits geometric details through a hierarchical object encoding paradigm, which comprises a positional encoding layer and a local reference frame encoding layer. For each point, we first encode its global position using a mini-PointNet [63], and then construct  $SE(3)$ -invariant local reference frame (**LRF**) to gather local descriptors. These two encodings complement each other, as the local descriptors capture fine geometric structures within small neighborhoods, while the positional encoding layer offers global geometric context. Leveraging  $\tilde{\mathbf{Q}}^f$  for example, the process of constructing LRF encoding is as follows. For each point  $\tilde{\mathbf{q}}^m$  in  $\tilde{\mathbf{Q}}^f$ , we build a local region set  $\tilde{\mathcal{Q}}^m = \{\tilde{\mathbf{q}}_j, \text{ where } \|\tilde{\mathbf{q}}_j - \tilde{\mathbf{q}}^m\|_2 \leq r\}_{j=1}^{N_D}$  by grouping  $N_D$  neighboring points of  $\tilde{\mathbf{q}}^m$ . The transformation pose  $\{\mathbf{R}_L^m, \mathbf{t}_L^m, s_L^m\}$  for LRF is computed similarly to GRF (Eq. 3, 4, 5), except that LRF is built upon a local point set while GRF is based on the entire point cloud. By computing the transformation pose, we calculate local point descriptors as

$$\mathcal{Q}_L^m = \tilde{\mathcal{Q}}_L^m = \{(\mathbf{R}_L^m)^\top (\tilde{\mathbf{q}}_j - \mathbf{t}_L^m) / s_L^m\}_{j=1}^{N_D}, \quad (8)$$

$$\mathcal{Q}_L^f = \{\mathcal{Q}_L^m\}_{m=1}^{N^f}.$$

Similarly, we transform  $\mathbf{P}^f$  to  $\mathbf{P}_L^f$ . Note that  $Q_L^m = \tilde{Q}_L^m$  since LRF is pose-invariant. Then, the LRF encoding is extracted from  $\mathbf{Q}_L^f$  and  $\mathbf{P}_L^f$  with a three-layer MLP.

Positional encoding and LRF encoding are combined with the geometric and color features as the input of the Geometric Transformer. Similar to initial pose prediction, by decoding these features, we obtain the fine point-wise features  $\hat{F}_Q^f, \hat{F}_P^f$  and overlap confidences  $\hat{O}_Q^f, \hat{O}_P^f$ , which are then used to obtain the overlap-aware fine correlation matrix  $\mathbf{X}^f \in \mathbb{R}^{(N^f+1) \times (N^f+1)}$ . The final pose  $\Delta\mathbf{T}$  is predicted by solving Eq. (1) using  $\mathbf{X}^f$  with the weighted SVD algorithm.

## 4. Experiments

### 4.1. Experimental Setup

**Implementation Details.** Implemented with PyTorch [60], we use the DINOv2 [12, 58] pre-trained ViT-base [15] backbone to encode color information. GeoTransformers [64] with attention [73] and sparse-to-dense linear attention [46] are respectively employed to extract coarse and fine geometric correspondences. The network is trained with standard MegaPose synthetic dataset [37] for BOP unseen object pose estimation track [28]. It contains over 2 million images of around 50K objects selected from Google Scanned Objects [16] and ShapeNet [5]. We set the training epochs to 3 with a batch size of 32 on 4 RTX 3090 GPUs. The network is trained with Adam [33] and cosine annealing [51], using a base learning rate of  $10^{-4}$ . Moreover, we leverage InfoNCE [57] loss to constrain the learning of correlation matrix and weighted BCE loss for supervising overlap prediction.

**Datasets and Benchmarks.** We evaluate our method on BOP test split [27] of three different real-world datasets: LM-O [2], TUD-L [26], and YCB-V [81]. *LM-O* consists of 200 images from one clutter scene, where eight objects with occlusion are provided for testing. *TUD-L* comprises three moving objects with mild occlusion and diverse lighting conditions. *YCB-V* is very challenging due to severe occlusions and sensor noise. It comprises 900 testing images from 12 scenes consisting of 21 objects. For each query object in the test split, we randomly select a reference object beyond the test set (in the training or evaluation set). Unless specified, we constrain the maximal rotation difference between reference and target to  $50^\circ$  to ensure the ground-truth correspondence set is not empty. Moreover, the occlusion ratio of reference objects is required to be less than 30%.

**Evaluation Metrics.** For evaluating instance segmentation, we follow [27] to use the mean Average Precision (mAP) metric, which is computed across different Intersection-over-Union (IoU) thresholds (0.5 to 0.95, with a step size of 0.05). Only annotated instances with at least 10% projected visible surfaces are considered for evaluation. For object pose evaluation, we use the symmetry-aware BOP metric [27].

It is calculated as the mean of the Average Recall of three metrics, *i.e.*, Visible Surface Discrepancy (VSD), Maximum Symmetry-Aware Surface Distance (MSSD), and Maximum Symmetry-Aware Projection Distance (MSPD). Details of these metrics are explained in [27].

### 4.2. UNO Object Segmentation and Pose Estimation Results

**UNO Object Segmentation Results.** We compare our UNOSeg with some existing CAD-model-based unseen object segmentation methods [7, 46, 54] in Tab. 1. Leveraging a single image as a reference, our UNOSeg achieves comparable results with state-of-the-art methods (Ours 54.2% vs. SAM-6D 54.5%) at a faster speed (Ours 2.68s vs. SAM-6D 4.53s). Notably, UNOSeg-FastSAM achieves the best performance on YCB-V (mAP 67.3%). Compared to FastSAM [93], SAM [34] achieves consistently better results on three datasets. Therefore, we choose UNOSeg-SAM as the default segmentation for subsequent experiments.

**UNO Object Pose Estimation Results.** Since we are the first to conduct relative 6DoF pose estimation for unseen objects and build a brand-new benchmark, we re-implement some traditional [17, 65, 89] and learning-based methods [4, 10, 11, 46, 62] for comparison. **Note that we leverage identical data pre-processing, segmentation, and evaluation protocols for all methods for fair comparison.** Moreover, we also compare UNOPose with two CAD-model-based pose estimators leveraging  $SE(3)$ -invariant PPF feature [1, 35]. All results are illustrated in Tab. 2. It clearly shows that our method surpasses all image-reference-based methods by a large margin, and even achieves comparable results with CAD-model-based methods using class-specific detectors [22, 47] (Ours 70.9% vs. ZTE-PPF [1] 69.0% vs. Koenig-PPF [35] 75.1%). ‘‘Ref. AlignCenter’’ directly uses the rotation of reference as prediction, meanwhile leveraging the shift between center points of query and reference as relative translation, so it can be regarded as the baseline of all methods. Among all traditional descriptors, PPF with Iterative Closest Point (ICP) refinement [17] achieves the best results (AR 46.9%). Learning-based methods demonstrate varying generalization abilities on unseen objects. For example, the GeoTransformer-based method UTOPIC, designed for registering object-level partial point clouds, performs suboptimally in our setting. In contrast, the adapted unseen object pose estimation methods, *i.e.* SAM-6D [46] and FreeZe [4], achieve satisfactory results compared to their counterparts.

**Run-time Analysis.** Evaluated on a single RTX 3090 GPU, our pipeline runs at 3.70s for one image, including 2.68s for segmentation and 1.02s for pose estimation (Tab. 1 - 2).

Method	Seg. Model	Modality	CAD model	LM-O	TUD-L	YCB-V	Avg	Time (s)
ZeroPose [7]	SAM [34]	RGB	✓	35.6	42.1	53.4	43.7	3.90
CNOS [54]	FastSAM [93]	RGB	✓	39.7	48.0	59.9	49.2	<b>0.23</b>
CNOS [54]	SAM [34]	RGB	✓	39.6	39.1	59.5	46.1	1.71
SAM-6D [46]	FastSAM [93]	RGB-D	✓	<u>42.2</u>	51.7	62.1	52.0	1.47
SAM-6D [46]	SAM [34]	RGB-D	✓	<b>46.0</b>	<b>56.9</b>	60.5	<b>54.5</b>	4.53
<b>UNOSeg (Ours)</b>	FastSAM [93]	RGB	✗	37.3	50.3	<b>67.3</b>	51.6	<u>0.24</u>
<b>UNOSeg (Ours)</b>	SAM [34]	RGB	✗	39.7	<u>56.2</u>	<u>66.8</u>	<u>54.2</u>	2.68

Table 1. **Segmentation results (mAP) on LM-O, TUD-L, and YCB-V datasets.** Results of other methods are obtained from the BOP website [bop.felk.cvut.cz/leaderboards/segmentation-unseen-bop23](http://bop.felk.cvut.cz/leaderboards/segmentation-unseen-bop23). For each column, we denote the best score in **bold** and the second best score with underline.

Method	Seg. Model	Modality	Ref. Type	LM-O	TUD-L	YCB-V	Avg	Time (s)
ZTE-PPF [1]	MRCNN [22]	D	Model	<b>66.3</b>	90.4	50.2	69.0	<b>0.74</b>
Koenig-PPF [35]	Retina/MRCNN	RGB-D	Model	63.1	<b>92.0</b>	<b>70.1</b>	<b>75.1</b>	0.99
Ref. AlignCenter	UNOSeg-SAM	D	Image	27.3	28.8	47.5	34.5	2.69
FPFH+RANSAC [65]	UNOSeg-SAM	D	Image	31.0	31.0	50.0	37.3	6.38
FPFH+MAC [89]	UNOSeg-SAM	D	Image	22.5	22.1	49.6	31.4	136.94
PPF [17]	UNOSeg-SAM	D	Image	29.7	14.8	38.3	27.6	11.79
PPF_3D_ICP [17]	UNOSeg-SAM	D	Image	44.7	29.1	66.8	46.9	14.27
FCGF+RANSAC [11]	UNOSeg-SAM	D	Image	38.9	59.0	57.6	51.8	10.96
FCGF+MAC [89]	UNOSeg-SAM	D	Image	33.9	48.3	51.0	44.4	60.53
UTOPIC [10]	UNOSeg-SAM	D	Image	13.7	35.4	10.5	19.9	4.00
GeDi [62]	UNOSeg-SAM	D	Image	42.8	67.3	60.6	56.9	48.89
FreeZe [4]	UNOSeg-SAM	RGB-D	Image	45.5	68.3	65.5	59.8	52.96
SAM-6D* [46]	UNOSeg-SAM	RGB-D	Posed Image	54.5	29.7	68.1	50.8	4.21
<b>UNOPose (Ours)</b>	UNOSeg-FastSAM	RGB-D	Image	55.8	66.5	81.9	68.1	<b>1.11</b>
<b>UNOPose (Ours)</b>	UNOSeg-SAM	RGB-D	Image	<b>58.7</b>	<b>71.0</b>	<b>83.1</b>	<b>70.9</b>	3.70

Table 2. **Pose estimation results on LM-O, TUD-L, and YCB-V datasets.** The mean Average Recall (%) of the BOP metric and the average time (s) per image are reported. We highlight the best scores of each setting in **bold**. Specifically, for adapting SAM-6D [46] to our setting, we randomly choose one of the two templates which [46] uses as a canonical reference.

### 4.3. One Reference for a Category

To minimize the efforts of acquiring references, we leverage a single reference for all objects of the same category in a dataset. Tab. 3 illustrates the qualitative and quantitative experimental results on TUD-L. It is worth noting that the target object in TUD-L is dynamic rather than static, preventing methods from leveraging background information. This setup poses challenges for relative pose estimation methods that rely on scene features, making them likely to fail in this task. Despite this, UNOPose achieves impressive performance (60.7% in terms of the  $AR_{BOP}$  metric) with only a single reference per category. The visualization results in Tab. 3b further show UNOPose is capable of predicting omnidirectional relative poses. Additional experiments on reference selection are provided in the supplementary material.

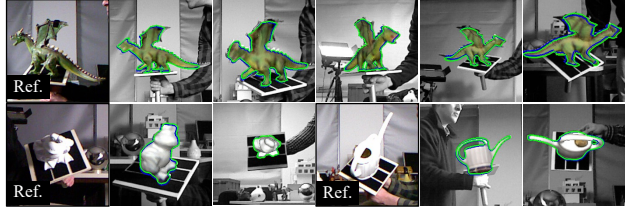
### 4.4. Ablation Studies

We ablate some key ingredients in UNOPose and present the results in Tab. 4, Tab. 5 and Fig. 3.

**Effectiveness of GRF and LRF.** As demonstrated in Sec. 3.3.2, GRF transfers arbitrary object poses to an  $SE(3)$ -invariant frame, while LRF assists with extracting precise local descriptors for fine pose estimation. Tab. 4 shows that the effectiveness of GRF and LRF is complementary in UNOPose. Specifically, GRF brings significant performance enhancement in the coarse pose estimation (Tab. 4 A1 vs. A0, A3 vs. A2), providing an accurate pose initialization for the next stage. Meanwhile, LRF is constructed to exploit fine-grained local information, primarily enhancing the fine pose estimation results (Tab. 4 B0 vs. B2, B1 vs. B3). With both GRF and LRF, our network achieves obvious performance improvement against the counterpart (Tab. 4 A3 vs. A0, B3 vs. B0).

Category	VSD	MSSD	MSPD	AR <sub>BOP</sub>
Dragon	47.1	73.2	69.4	63.2
Frog	59.4	52.6	57.6	56.4
Can	56.8	65.6	65.2	62.5
Avg	<b>54.4</b>	<b>63.7</b>	<b>64.1</b>	<b>60.7</b>

(a)



(b)

Table 3. **One reference per category experiments on TUD-L.** Blue and green contours denote ground-truth and estimated poses, respectively.

ROW	GRF	LRF	FPE	VSD	MSSD	MSPD	AR <sub>BOP</sub>
A0	✗	✗	✗	64.6	68.1	59.2	63.9
A1	✓	✗	✗	66.4	72.8	63.2	67.5
A2	✗	✓	✗	66.2	69.5	60.4	65.4
A3	✓	✓	✗	66.9	73.2	63.5	67.9
B0	✗	✗	✓	79.8	85.0	75.5	80.1
B1	✓	✗	✓	79.4	85.2	76.6	80.4
B2	✗	✓	✓	<b>81.1</b>	85.1	76.6	80.9
B3	✓	✓	✓	80.7	<b>86.0</b>	<b>77.7</b>	<b>81.5</b>

Table 4. **Ablation of GRF and LRF on YCB-V.** FPE stands for “fine pose estimation”.

ROW	Method	VSD	MSSD	MSPD	AR <sub>BOP</sub>
C0	B3 + Soft Correspondence [84]	77.1	81.7	72.7	77.2
C1	B3 + Overlap Predictor	<b>82.6</b>	<b>87.4</b>	<b>79.4</b>	<b>83.1</b>
D0	C1: Seg. → CNOS [54]	77.4	80.9	73.6	77.3
D1	C1: Seg. → SAM-6D [46]	78.3	82.1	74.3	78.2
D2	C1: Seg. → MRCNN [22, 36]	81.2	85.7	77.9	81.6
D3	C1: Seg. → GT Seg.	<b>86.6</b>	<b>89.2</b>	<b>82.1</b>	<b>86.0</b>

Table 5. **Ablation of overlap predictor and segmentation on YCB-V.**

**Ablation on Correspondence Loss.** In partial-to-partial point cloud registration, only some of the points can find their counterparts on the target point cloud. Therefore, the introduction of overlap prediction helps to distinguish the points in the overlap region and achieves good results (Tab. 5 C1 vs. Tab. 4 B3). Moreover, we consider soft correspondence loss in [84] as an alternative, which predicts probabilities of overlap between each point pair. However, the result did not meet the desired expectations (Tab. 5 C0).

**Ablation on Segmentation.** Tab. 1 showcases the advantage of our UNOSeg over other segmentation methods on YCB-V. Furthermore, substituting UNOSeg with CNOS [54], SAM-6D [46], or MRCNN [22, 36] results in a noticeable decline in UNOPose’s performance (Tab. 5 D0–D2). Moreover, substituting UNOSeg with ground-truth segmentation

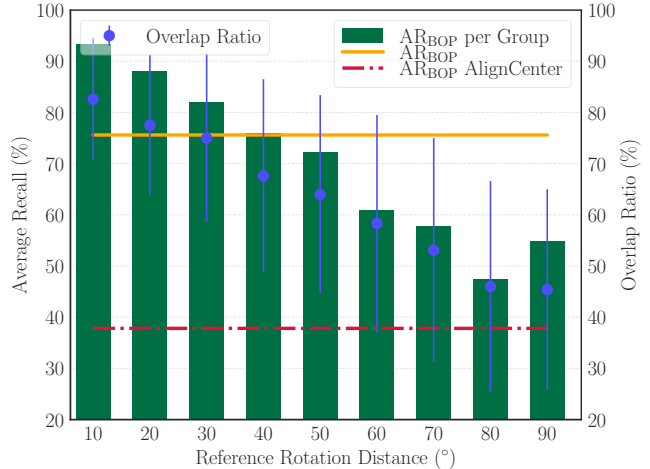


Figure 3. **Ablation of initial rotation distance between query and reference objects.** We categorize all testing objects into nine groups according to the initial rotation distance, and evaluate the AR<sub>BOP</sub> metric and overlap ratio for each group separately.

brings  $\approx 3\%$  performance enhancement (Tab. 5 D3 vs. C1).

**Ablation on Reference Rotation Distance.** To investigate the impact of the initial rotation distance between the query and reference images, we randomly select the reference object with a maximum rotation distance of  $90^\circ$  for each query object. Further, all testing objects are categorized into nine groups according to initial reference rotation distance. We separately evaluate each group and present the results in Fig. 3. Meanwhile, we calculate the overlap ratio between reference and query instances of each group and visualize the mean and standard deviation. Notably, performance significantly decreases when the rotation distance exceeds  $50^\circ$ . This decline is attributed to the reduced overlap between query and reference viewpoints. However, our network still shows favorable transfer ability in extreme relative pose estimation (rotation distance ( $80^\circ$ ,  $90^\circ$ ), overlap ratio 45.4%, AR<sub>BOP</sub> 54.8%).

The supplementary material presents further implementation details, visualization results, and more experimental analysis on reference selection and extensive datasets.



## 5. Conclusion, Limitation and Future work

This work has introduced UNOPose, a new approach for unseen object pose estimation with one reference. The key idea is constructing the  $SE(3)$ -invariant reference frame for tackling diverse pose and size variations. Moreover, we propose an overlap predictor for handling low-overlap scenarios. To evaluate the proposed method, we devise a new benchmark based on the BOP challenge and compare some state-of-the-art methods. Experimental results show UNOPose surpasses all compared reference-based methods significantly, and is competitive with some  $SE(3)$ -invariant-feature-based methods relying on CAD models.

**Limitation and Future Work.** While efficient, correspondence-based methods rely on predicting robust and dense correspondence between query and reference objects, thereby limited in extreme two-view geometry applications. Future work will focus on reconstructing the unseen object from a single reference [48, 94] and concurrently estimating its object pose.

## References

- [1] Anonymous. Zte-ppf. [https://bop.felk.cvut.cz/method\\_info/250/](https://bop.felk.cvut.cz/method_info/250/), 2022. 2, 6, 7
- [2] Eric Brachmann, Alexander Krull, Frank Michel, Stefan Gumhold, Jamie Shotton, and Carsten Rother. Learning 6D object pose estimation using 3D object coordinates. In *ECCV*, 2014. 2, 6
- [3] Dingding Cai, Janne Heikkilä, and Esa Rahtu. Ove6d: Object viewpoint encoding for depth-based 6d object pose estimation. In *CVPR*, pages 6803–6813, 2022. 1, 2, 3
- [4] Andrea Caraffa, Davide Boscaini, Amir Hamza, and Fabio Poiesi. Freeze: Training-free zero-shot 6d pose estimation with geometric and vision foundation models. In *ECCV*, 2024. 3, 6, 7
- [5] Angel X Chang, Thomas Funkhouser, Leonidas Guibas, Pat Hanrahan, Qixing Huang, Zimo Li, Silvio Savarese, Manolis Savva, Shuran Song, Hao Su, et al. ShapeNet: An information-rich 3D model repository. *arXiv preprint arXiv:1512.03012*, 2015. 6
- [6] Dengsheng Chen, Jun Li, Zheng Wang, and Kai Xu. Learning canonical shape space for category-level 6D object pose and size estimation. In *CVPR*, pages 11970–11979, 2020. 1, 3
- [7] Jianqiu Chen, Zikun Zhou, Mingshan Sun, Rui Zhao, Liwei Wu, Tianpeng Bao, and Zhenyu He. Zeropose: Cad-prompted zero-shot object 6d pose estimation in cluttered scenes. *IEEE TCSVT*, 2024. 4, 6, 7
- [8] Kai Chen and Qi Dou. SGPA: Structure-guided prior adaptation for category-level 6D object pose estimation. In *ICCV*, pages 2773–2782, 2021. 3
- [9] Wei Chen, Xi Jia, Hyung Jin Chang, Jinming Duan, Shen Linlin, and Ales Leonardis. FS-Net: Fast shape-based network for category-level 6D object pose estimation with decoupled rotation mechanism. In *CVPR*, pages 1581–1590, 2021. 3
- [10] Zhilei Chen, Honghua Chen, Lina Gong, Xuefeng Yan, Jun Wang, Yanwen Guo, Jing Qin, and Mingqiang Wei. Utopic: Uncertainty-aware overlap prediction network for partial point cloud registration. In *Computer Graphics Forum*, pages 87–98. Wiley Online Library, 2022. 6, 7
- [11] Christopher Choy, Jaesik Park, and Vladlen Koltun. Fully convolutional geometric features. In *ICCV*, pages 8958–8966, 2019. 3, 6, 7
- [12] Timothée Darcet, Maxime Oquab, Julien Mairal, and Piotr Bojanowski. Vision transformers need registers. In *ICLR*, 2024. 6
- [13] Haowen Deng, Tolga Birdal, and Slobodan Ilic. Ppf-foldnet: Unsupervised learning of rotation invariant 3d local descriptors. In *ECCV*, pages 602–618, 2018. 3
- [14] Haowen Deng, Tolga Birdal, and Slobodan Ilic. Ppfnet: Global context aware local features for robust 3d point matching. In *CVPR*, pages 195–205, 2018. 3
- [15] Alexey Dosovitskiy, Lucas Beyer, Alexander Kolesnikov, Dirk Weissenborn, Xiaohua Zhai, Thomas Unterthiner, Mostafa Dehghani, Matthias Minderer, Georg Heigold, Sylvain Gelly, et al. An image is worth 16x16 words: Transformers for image recognition at scale. In *ICLR*, 2021. 6
- [16] Laura Downs, Anthony Francis, Nate Koenig, Brandon Kinman, Ryan Hickman, Krista Reymann, Thomas B McHugh, and Vincent Vanhoucke. Google scanned objects: A high-quality dataset of 3d scanned household items. In *ICRA*, pages 2553–2560. IEEE, 2022. 6
- [17] Bertram Drost, Markus Ulrich, Nassir Navab, and Slobodan Ilic. Model globally, match locally: Efficient and robust 3d object recognition. In *CVPR*, pages 998–1005. Ieee, 2010. 3, 6, 7
- [18] Guoguang Du, Kai Wang, Shiguo Lian, and Kaiyong Zhao. Vision-based robotic grasping from object localization, object pose estimation to grasp estimation for parallel grippers: a review. *Artificial Intelligence Review*, 54(3):1677–1734, 2021. 1
- [19] Zhaoxin Fan, Zhenbo Song, Jian Xu, Zhicheng Wang, Kejian Wu, Hongyan Liu, and Jun He. Object level depth reconstruction for category level 6d object pose estimation from monocular rgb image. In *ECCV*, pages 220–236. Springer, 2022. 3
- [20] Andrea Frome, Daniel Huber, Ravi Kolluri, Thomas Bülow, and Jitendra Malik. Recognizing objects in range data using regional point descriptors. In *ECCV*, pages 224–237. Springer, 2004. 5
- [21] Rasmus Laurvig Haugaard and Anders Glent Buch. Surfemb: Dense and continuous correspondence distributions for object pose estimation with learnt surface embeddings. In *CVPR*, pages 6749–6758, 2022. 3, 5
- [22] Kaiming He, Georgia Gkioxari, Piotr Dollár, and Ross Girshick. Mask R-CNN. In *ICCV*, pages 2961–2969, 2017. 6, 7, 8
- [23] Xingyi He, Jiaming Sun, Yuang Wang, Di Huang, Hujun Bao, and Xiaowei Zhou. Onepose++: Keypoint-free one-shot object pose estimation without cad models. *NeurIPS*, 35: 35103–35115, 2022. 1, 3
- [24] Yisheng He, Haibin Huang, Haoqiang Fan, Qifeng Chen, and Jian Sun. Ffb6d: A full flow bidirectional fusion network for 6d pose estimation. In *CVPR*, pages 3003–3013, 2021. 3

- [25] Yisheng He, Yao Wang, Haoqiang Fan, Jian Sun, and Qifeng Chen. Fs6d: Few-shot 6d pose estimation of novel objects. In *CVPR*, pages 6814–6824, 2022. 1
- [26] Tomas Hodan, Frank Michel, Eric Brachmann, Wadim Kehl, Anders GlentBuch, Dirk Kraft, Bertram Drost, Joel Vidal, Stephan Ihrke, Xenophon Zabulis, et al. BOP: Benchmark for 6D Object Pose Estimation. In *ECCV*, pages 19–34, 2018. 2, 6
- [27] Tomas Hodan, Martin Sundermeyer, Bertram Drost, Yann Labbe, Eric Brachmann, Frank Michel, Carsten Rother, and Jiri Matas. BOP Challenge 2020 on 6D object localization. In *ECCVW*, pages 577–594, 2020. 6
- [28] Tomas Hodan, Martin Sundermeyer, Yann Labbe, Van Nguyen Nguyen, Gu Wang, Eric Brachmann, Bertram Drost, Vincent Lepetit, Carsten Rother, and Jiri Matas. Bop challenge 2023 on detection, segmentation and pose estimation of seen and unseen rigid objects. In *CVPRW*, 2024. 2, 6
- [29] Yinlin Hu, Pascal Fua, Wei Wang, and Mathieu Salzmann. Single-stage 6d object pose estimation. In *CVPR*, pages 2930–2939, 2020. 3
- [30] Junwen Huang, Hao Yu, Kuan-Ting Yu, Nassir Navab, Slobodan Ilic, and Benjamin Busam. Matchu: Matching unseen objects for 6d pose estimation from rgb-d images. In *CVPR*, 2024. 3
- [31] Siyuan Huang, Siyuan Qi, Yinxue Xiao, Yixin Zhu, Ying Nian Wu, and Song-Chun Zhu. Cooperative holistic scene understanding: Unifying 3d object, layout, and camera pose estimation. *NeurIPS*, 31, 2018. 1
- [32] Shengyu Huang, Zan Gojcic, Mikhail Usvyatsov, Andreas Wieser, and Konrad Schindler. Predator: Registration of 3d point clouds with low overlap. In *CVPR*, pages 4267–4276, 2021. 3
- [33] Diederik P. Kingma and Jimmy Ba. Adam: A method for stochastic optimization. In *ICLR*, 2015. 6
- [34] Alexander Kirillov, Eric Mintun, Nikhila Ravi, Hanzi Mao, Chloe Rolland, Laura Gustafson, Tete Xiao, Spencer Whitehead, Alexander C Berg, Wan-Yen Lo, et al. Segment anything. In *ICCV*, pages 4015–4026, 2023. 2, 4, 6, 7
- [35] Rebecca König and Bertram Drost. A hybrid approach for 6dof pose estimation. In *ECCV*, pages 700–706. Springer, 2020. 2, 6, 7
- [36] Yann Labbé, Justin Carpentier, Mathieu Aubry, and Josef Sivic. CosyPose: Consistent multi-view multi-object 6D pose estimation. In *ECCV*, pages 574–591, 2020. 1, 8
- [37] Yann Labbé, Lucas Manuelli, Arsalan Mousavian, Stephen Tyree, Stan Birchfield, Jonathan Tremblay, Justin Carpentier, Mathieu Aubry, Dieter Fox, and Josef Sivic. Megapose: 6d pose estimation of novel objects via render & compare. In *CoRL*, pages 715–725. PMLR, 2023. 1, 2, 3, 6
- [38] Junha Lee, Seungwook Kim, Minsu Cho, and Jaesik Park. Deep hough voting for robust global registration. In *ICCV*, pages 15994–16003, 2021. 3
- [39] Jiahao Li, Changhao Zhang, Ziyao Xu, Hangning Zhou, and Chi Zhang. Iterative distance-aware similarity matrix convolution with mutual-supervised point elimination for efficient point cloud registration. In *ECCV*, pages 378–394. Springer, 2020. 3
- [40] Xiaolong Li, Yijia Weng, Li Yi, Leonidas J Guibas, A Abbott, Shuran Song, and He Wang. Leveraging se (3) equivariance for self-supervised category-level object pose estimation from point clouds. *NeurIPS*, 34, 2021. 5
- [41] Yi Li, Gu Wang, Xiangyang Ji, Yu Xiang, and Dieter Fox. DeepIM: Deep iterative matching for 6D pose estimation. *IJCV*, 128(3):657–678, 2020. 3
- [42] Zhigang Li, Gu Wang, and Xiangyang Ji. CDPN: Coordinates-Based Disentangled Pose Network for Real-Time RGB-Based 6-DoF Object Pose Estimation. In *ICCV*, pages 7678–7687, 2019. 1, 3
- [43] Amy Lin, Jason Y Zhang, Deva Ramanan, and Shubham Tulsiani. Relpose++: Recovering 6d poses from sparse-view observations. In *3DV*, 2024. 3
- [44] Jiehong Lin, Zewei Wei, Zhihao Li, Songcen Xu, Kui Jia, and Yuanqing Li. DualPoseNet: Category-level 6D object pose and size estimation using dual pose network with refined learning of pose consistency. In *ICCV*, pages 3560–3569, 2021. 3
- [45] Jiehong Lin, Zewei Wei, Changxing Ding, and Kui Jia. Category-level 6d object pose and size estimation using self-supervised deep prior deformation networks. In *ECCV*, pages 19–34, 2022. 3
- [46] Jiehong Lin, Lihua Liu, Dekun Lu, and Kui Jia. Sam-6d: Segment anything model meets zero-shot 6d object pose estimation. In *CVPR*, 2024. 1, 3, 4, 5, 6, 7, 8
- [47] Tsung-Yi Lin, Priya Goyal, Ross Girshick, Kaiming He, and Piotr Dollár. Focal loss for dense object detection. In *ICCV*, pages 2980–2988, 2017. 6
- [48] Ruoshi Liu, Rundi Wu, Basile Van Hoorick, Pavel Tokmakov, Sergey Zakharov, and Carl Vondrick. Zero-1-to-3: Zero-shot one image to 3d object. In *ICCV*, pages 9298–9309, 2023. 3, 9
- [49] Xingyu Liu, Gu Wang, Yi Li, and Xiangyang Ji. CATRE: iterative point clouds alignment for category-level object pose refinement. In *ECCV*, 2022. 3
- [50] Yuan Liu, Yilin Wen, Sida Peng, Cheng Lin, Xiaoxiao Long, Taku Komura, and Wenping Wang. Gen6d: Generalizable model-free 6-dof object pose estimation from rgb images. In *ECCV*, 2022. 1, 2
- [51] Ilya Loshchilov and Frank Hutter. SGDR: stochastic gradient descent with warm restarts. In *ICLR*, 2017. 6
- [52] Eric Marchand, Hideaki Uchiyama, and Fabien Spindler. Pose estimation for augmented reality: a hands-on survey. *IEEE TVCG*, 22(12):2633–2651, 2015. 1
- [53] Van Nguyen Nguyen, Yinlin Hu, Yang Xiao, Mathieu Salzmann, and Vincent Lepetit. Templates for 3d object pose estimation revisited: Generalization to new objects and robustness to occlusions. In *CVPR*, pages 6771–6780, 2022. 3
- [54] Van Nguyen Nguyen, Thibault Groueix, Georgy Ponimatkin, Vincent Lepetit, and Tomas Hodan. Cnos: A strong baseline for cad-based novel object segmentation. In *ICCV*, pages 2134–2140, 2023. 1, 3, 4, 6, 7, 8
- [55] Van Nguyen Nguyen, Thibault Groueix, Mathieu Salzmann, and Vincent Lepetit. Gigapose: Fast and robust novel object pose estimation via one correspondence. In *CVPR*, 2024. 1, 3

- [56] Yinyu Nie, Xiaoguang Han, Shihui Guo, Yujian Zheng, Jian Chang, and Jian Jun Zhang. Total3DUnderstanding: Joint layout, object pose and mesh reconstruction for indoor scenes from a single image. In *CVPR*, pages 55–64, 2020. 1
- [57] Aaron van den Oord, Yazhe Li, and Oriol Vinyals. Representation learning with contrastive predictive coding. *arXiv preprint arXiv:1807.03748*, 2018. 6
- [58] Maxime Oquab, Timothée Darcet, Théo Moutakanni, Huy V. Vo, Marc Szafraniec, Vasil Khalidov, Pierre Fernandez, Daniel HAZIZA, Francisco Massa, Alaaeldin El-Nouby, Mido Assran, Nicolas Ballas, Wojciech Galuba, Russell Howes, Po-Yao Huang, Shang-Wen Li, Ishan Misra, Michael Rabbat, Vasu Sharma, Gabriel Synnaeve, Hu Xu, Herve Jegou, Julien Mairal, Patrick Labatut, Armand Joulin, and Piotr Bojanowski. DINOv2: Learning robust visual features without supervision. *TMLR*, 2024. 2, 3, 4, 5, 6
- [59] Evin Pinar Örnek, Yann Labbé, Bugra Tekin, Lingni Ma, Cem Keskin, Christian Forster, and Tomas Hodan. Foundpose: Unseen object pose estimation with foundation features. In *CVPR*, 2024. 3
- [60] Adam Paszke, Sam Gross, Francisco Massa, Adam Lerer, James Bradbury, Gregory Chanan, Trevor Killeen, Zeming Lin, Natalia Gimelshein, Luca Antiga, et al. PyTorch: An imperative style, high-performance deep learning library. In *NeurIPS*, pages 8026–8037, 2019. 6
- [61] Sida Peng, Yuan Liu, Qixing Huang, Xiaowei Zhou, and Hujun Bao. Pynet: Pixel-wise voting network for 6dof pose estimation. In *CVPR*, pages 4561–4570, 2019. 1, 3
- [62] Fabio Poiesi and Davide Boscaini. Learning general and distinctive 3d local deep descriptors for point cloud registration. *IEEE TPAMI*, 45(3):3979–3985, 2022. 3, 6, 7
- [63] Charles R Qi, Hao Su, Kaichun Mo, and Leonidas J Guibas. PointNet: Deep learning on point sets for 3D classification and segmentation. *CVPR*, 1(2):4, 2017. 5
- [64] Zheng Qin, Hao Yu, Changjian Wang, Yulan Guo, Yuxing Peng, Slobodan Ilic, Dewen Hu, and Kai Xu. Geotransformer: Fast and robust point cloud registration with geometric transformer. *IEEE TPAMI*, 2023. 3, 5, 6
- [65] Radu Bogdan Rusu, Nico Blodow, and Michael Beetz. Fast point feature histograms (fpfh) for 3d registration. In *ICRA*, pages 3212–3217. IEEE, 2009. 3, 6, 7
- [66] Ivan Shugurov, Sergey Zakharov, and Slobodan Ilic. Dpodv2: Dense correspondence-based 6 dof pose estimation. *IEEE TPAMI*, 44(11):7417–7435, 2021. 3
- [67] Ivan Shugurov, Fu Li, Benjamin Busam, and Slobodan Ilic. Osop: A multi-stage one shot object pose estimation framework. In *CVPR*, pages 6835–6844, 2022. 3
- [68] Fridtjof Stein, Gérard Medioni, et al. Structural indexing: Efficient 3-d object recognition. *IEEE TPAMI*, 14(2):125–145, 1992. 5
- [69] Yongzhi Su, Jason Rambach, Nareg Minaskan, Paul Lesur, Alain Pagani, and Didier Stricker. Deep multi-state object pose estimation for augmented reality assembly. In *IEEE International Symposium on Mixed and Augmented Reality Adjunct (ISMAR-Adjunct)*, pages 222–227, 2019. 1
- [70] Jiaming Sun, Zihao Wang, Siyu Zhang, Xingyi He, Hongcheng Zhao, Guofeng Zhang, and Xiaowei Zhou. Onepose: One-shot object pose estimation without cad models. In *CVPR*, pages 6825–6834, 2022. 1, 2, 3
- [71] Meng Tian, Marcelo H Ang Jr, and Gim Hee Lee. Shape prior deformation for categorical 6D object pose and size estimation. In *ECCV*, 2020. 1, 3
- [72] Jonathan Tremblay, Thang To, Balakumar Sundaralingam, Yu Xiang, Dieter Fox, and Stan Birchfield. Deep object pose estimation for semantic robotic grasping of household objects. In *CoRL*, pages 306–316, 2018. 1
- [73] Ashish Vaswani, Noam Shazeer, Niki Parmar, Jakob Uszkoreit, Llion Jones, Aidan N. Gomez, Lukasz Kaiser, and Illia Polosukhin. Attention is all you need. In *NeurIPS*, pages 5998–6008, 2017. 6
- [74] Chen Wang, Danfei Xu, Yuke Zhu, Roberto Martín-Martín, Cewu Lu, Li Fei-Fei, and Silvio Savarese. DenseFusion: 6D object pose estimation by iterative dense fusion. In *CVPR*, pages 3343–3352, 2019. 1, 3
- [75] Gu Wang, Fabian Manhardt, Federico Tombari, and Xiangyang Ji. GDR-Net: Geometry-guided direct regression network for monocular 6D object pose estimation. In *CVPR*, pages 16611–16621, 2021. 1, 3
- [76] He Wang, Srinath Sridhar, Jingwei Huang, Julien Valentin, Shuran Song, and Leonidas J Guibas. Normalized object coordinate space for category-level 6D object pose and size estimation. In *CVPR*, pages 2642–2651, 2019. 1, 3
- [77] Jiase Wang, Kai Chen, and Qi Dou. Category-level 6D object pose estimation via cascaded relation and recurrent reconstruction networks. In *IROS*, 2021. 1
- [78] Yue Wang and Justin M Solomon. Deep closest point: Learning representations for point cloud registration. In *ICCV*, pages 3523–3532, 2019. 3
- [79] Bowen Wen, Wei Yang, Jan Kautz, and Stan Birchfield. FoundationPose: Unified 6d pose estimation and tracking of novel objects. In *CVPR*, 2024. 1, 2, 3
- [80] Chin-Hsuan Wu, Yen-Chun Chen, Bolivar Solarte, Lu Yuan, and Min Sun. ifusion: Inverting diffusion for pose-free reconstruction from sparse views. *arXiv preprint arXiv:2312.17250*, 2023. 3
- [81] Yu Xiang, Tanner Schmidt, Venkatraman Narayanan, and Dieter Fox. PoseCNN: A convolutional neural network for 6D object pose estimation in cluttered scenes. *RSS*, 2018. 2, 6
- [82] Jiaqi Yang, Qian Zhang, Yang Xiao, and Zhiguo Cao. Toldi: An effective and robust approach for 3d local shape description. *PR*, 65:175–187, 2017. 3, 5
- [83] Yang You, Ruoxi Shi, Weiming Wang, and Cewu Lu. Cppf: Towards robust category-level 9d pose estimation in the wild. In *CVPR*, pages 6866–6875, 2022. 5
- [84] Hao Yu, Fu Li, Mahdi Saleh, Benjamin Busam, and Slobodan Ilic. Cofinet: Reliable coarse-to-fine correspondences for robust pointcloud registration. *NeurIPS*, 34, 2021. 8
- [85] Hao Yu, Zheng Qin, Ji Hou, Mahdi Saleh, Dongsheng Li, Benjamin Busam, and Slobodan Ilic. Rotation-invariant transformer for point cloud matching. In *CVPR*, pages 5384–5393, 2023. 5
- [86] Hao Yu, Ji Hou, Zheng Qin, Mahdi Saleh, Ivan Shugurov, Kai Wang, Benjamin Busam, and Slobodan Ilic. Riga: Rotation-

- invariant and globally-aware descriptors for point cloud registration. *IEEE TPAMI*, 46(5):3796–3812, 2024. 3
- [87] Jason Y Zhang, Deva Ramanan, and Shubham Tulsiani. Rel-pose: Predicting probabilistic relative rotation for single objects in the wild. In *ECCV*, pages 592–611. Springer, 2022. 2, 3
- [88] Ruida Zhang, Ziqin Huang, Gu Wang, Chenyangguang Zhang, Yan Di, Xingxing Zuo, Jiwen Tang, and Xiangyang Ji. Lapose: Laplacian mixture shape modeling for rgb-based category-level object pose estimation. In *ECCV*, 2024. 3
- [89] Xiyu Zhang, Jiaqi Yang, Shikun Zhang, and Yanning Zhang. 3d registration with maximal cliques. In *CVPR*, pages 17745–17754, 2023. 6, 7
- [90] Chen Zhao, Yinlin Hu, and Mathieu Salzmann. Fusing local similarities for retrieval-based 3d orientation estimation of unseen objects. In *ECCV*, pages 106–122. Springer, 2022. 3
- [91] Chen Zhao, Tong Zhang, and Mathieu Salzmann. 3d-aware hypothesis & verification for generalizable relative object pose estimation. In *ICLR*, 2023. 2, 3
- [92] Chen Zhao, Tong Zhang, Zheng Dang, and Mathieu Salzmann. Dvmnet: Computing relative pose for unseen objects beyond hypotheses. In *CVPR*, 2024. 2, 3
- [93] Xu Zhao, Wenchao Ding, Yongqi An, Yinglong Du, Tao Yu, Min Li, Ming Tang, and Jinqiao Wang. Fast segment anything. *arXiv preprint arXiv:2306.12156*, 2023. 6, 7
- [94] Zi-Xin Zou, Zhipeng Yu, Yuan-Chen Guo, Yangguang Li, Ding Liang, Yan-Pei Cao, and Song-Hai Zhang. Triplane meets gaussian splatting: Fast and generalizable single-view 3d reconstruction with transformers. In *CVPR*, pages 10324–10335, 2024. 9